SCIENCE CHINA
Earth Sciences

SPECIAL TOPIC: Remote Sensing and Global Change
• RESEARCH PAPER •

October 2014 Vol.57 No.10: 2283–2292
doi: 10.1007/s11430-014-4925-1

Suitability mapping of global wetland areas and validation with remotely sensed data

ZHU Peng[1,3] & GONG Peng[1,2,4*]

[1] *State Key Laboratory of Remote Sensing Science, Jointly Sponsored by Institute of Remote Sensing Applications, Chinese Academy of Sciences and Beijing Normal University, Beijing 100101, China;*
[2] *Center for Earth System Science, Tsinghua University, Beijing 100084, China;*
[3] *University of Chinese Academy of Sciences, Beijing 100049, China;*
[4] *Joint Center for Global Change Studies, Beijing 100875, China*

Received October 29, 2013; accepted February 24, 2014; published online Jnly 15, 2014

With increasing urbanization and agricultural expansion, large tracts of wetlands have been either disturbed or converted to other uses. To protect wetlands, accurate distribution maps are needed. However, because of the dramatic diversity of wetlands and difficulties in field work, wetland mapping on a large spatial scale is very difficult to do. Until recently there were only a few high resolution global wetland distribution datasets developed for wetland protection and restoration. In this paper, we used hydrologic and climatic variables in combination with Compound Topographic Index (CTI) data in modeling the average annual water table depth at 30 arc-second grids over the continental areas of the world except for Antarctica. The water table depth data were modeled without considering influences of anthropogenic activities. We adopted a relationship between potential wetland distribution and water table depth to develop the global wetland suitability distribution dataset. The modeling results showed that the total area of global wetland reached 3.316×10^7 km^2. Remote-sensing-based validation based on a compilation of wetland areas from multiple sources indicates that the overall accuracy of our product is 83.7%. This result can be used as the basis for mapping the actual global wetland distribution. Because the modeling process did not account for the impact of anthropogenic water management such as irrigation and reservoir construction over suitable wetland areas, our result represents the upper bound of wetland areas when compared with some other global wetland datasets. Our method requires relatively fewer datasets and has a higher accuracy than a recently developed global wetland dataset.

global wetland suitability distribution, water balance model, CTI, accuracy assessment

Citation: Zhu P, Gong P. 2014. Suitability mapping of global wetland areas and validation with remotely sensed data. Science China: Earth Sciences, 57: 2283−2292, doi: 10.1007/s11430-014-4925-1

Wetlands provide important ecosystem and economic services, including water quality improvement, soil conservation, carbon sequestration, biodiversity support, underground water stabilization, and flood abatement (Zedler and Kercher, 2005). With intensifying anthropogenic activities, almost half of the wetlands have been lost (OECD, 1996). An accurate wetland distribution map is the basis for wetland protection. In the middle 1990s, a wetland survey of 74% of continental United States and 24% of Alaska has been completed (Wilen and Bates, 1995). From data acquired with Landsat Multispectral Scanner (MSS), Thematic Mapper (TM), and Enhanced Thematic Mapper Plus (ETM+) and data from China Brazil Earth Resource Satellite, wetland maps covering the entire China have been produced between 1978 and 2008 (1978, 1990, 2000, and 2008) followed by change analysis and assessment of protection efficacy of

*Corresponding author (email: penggong@mail.tsinghua.edu.cn)

© Science China Press and Springer-Verlag Berlin Heidelberg 2014

Chinese protected wetland areas (Gong et al., 2010; Niu et al., 2009; Niu et al., 2012; Zheng et al., 2012). Meanwhile wetland dynamics and vegetation distribution over areas with abundant wetland resources like the Poyang Lake have been extensively studied (Dronova et al., 2011; Hui et al., 2008; Ji et al., 2007). Due to logistic difficulties in field works over wetland areas, large area wetland mapping is dependent primarily on remotely sensed images.

There are several global land cover products explicitly containing wetland categories. These include the IGBP-DISCover developed by U.S. Geological Survey (USGS) (Loveland et al., 2000), MOD12Q1 V004 Land Cover Data product developed by Boston University from Moderate Resolution Imaging Spectroradiometer (MODIS) (Friedl et al., 2002), GLC2000 developed by European Commission Joint Research Center (Bartholomé and Belward, 2005), the Global Land Cover by National Mapping Organizations (GLCNMO) developed by Japanese International Steering Committee for Global Mapping (Tateishi et al., 2011), and the Finer Resolution Observation and Monitoring of Global Land Cover (FROM GLC) developed by Tsinghua University with Landsat TM/ETM+ data (Gong et al., 2013). In addition, a comprehensive 1-km Global Lakes and Wetlands Database (GLWD) was built based on multiple wetland datasets (Lehner and Döll, 2004). However, all of these datasets were developed from different data sources with different classification schemes. There were extensive spatial disagreements on wetland distribution among these datasets. Particularly, a recent comparison of water related land cover types showed that wetland was the land cover type with the lowest agreement (Nakaegawa, 2012). Moreover, given the high seasonality and annual variation in wetland dynamics and limited availability in satellite data acquisition, wetland mapping based on remotely sensed data is still facing with great uncertainty.

The increasing recognition of the important role wetlands play in global water and carbon cycling led to more and more land surface model (LSM) development researchers to incorporate water and carbon processes in wetlands into their model schemes. A recent project of Wetland and Wetland CH_4 Intercomparison of Models Project (WETCHIMP), aiming at investigating our present ability to simulate large-scale wetland characteristics and corresponding CH4 emissions, compared 10 models, and eight of them ran at global scale. The result showed that there were extensive disagreements on wetland extent in both space and time. The wetland modeling results ranged from 2.7×10^6 to 8.17×10^7 km^2 (Melton et al., 2012). The practical value of these wetland datasets was also limited because of the coarse resolution and lack of global validation.

In this paper, we employed global Compound Topographic Index (CTI) dataset and the relation between wetland and water table depth to derive the suitability distribution of global wetlands. Considering the fact that coastal wetlands are vulnerable to the influence of tide and its unusual hydrological characteristics, we only focused on inland wetlands. In a previous research, a sub-grid run-off parameterization scheme had been proposed based on TOPMODEL which used CTI to represent the status of local water storage (expressed as deficit or saturation) (Habets and Saulnier, 2001). This parameterization scheme was then coupled with land surface models ISAB and ORCHIDEE, respectively, leading to an improvement in the modeling of the proportion of saturation area in each sub-grid (Decharme and Douville, 2006; Decharme and Douville, 2007; Ringeval et al., 2012). These methods offered a reference for us to construct a relation between water table depth and CTI, but the scale used in the earlier researches was still too coarse for wetland mapping. We used CTI derived from a higher resolution topography dataset with a one-layer water balance model. Then the average water table depth at 5 min resolution attained with hydrological model was downscaled to 30 arc-second by using CTI. Finally, we characterized the suitability distribution of global land surface wetland without accounting for the impact of human activities by selecting appropriate thresholds for the downscaled water table depth.

1 Global wetland suitability areas modeling

The modeling process was divided into two parts: (1) obtaining soil water content with a water balance model; and (2) determining wetland suitability areas based on water table depth. Required data include CTI derived from global digital elevation model (DEM), climatic data used to drive the water balance model, and wetland/no wetland distribution data for parameter calibration.

1.1 Datasets

From 60°S to 60°N, we used 1 km flow accumulation data HydroSHEDS (http://hydrosheds.cr.usgs.gov/) from USGS to calculate CTI based on eq. (1). The flow accumulation data HydroSHEDS were produced from Shuttle Radar Topographic Mission (SRTM) DEM data through some post-processing to eliminate dams and false sinks and reduce errors caused by interpolation. For areas above 60°N, the CTI was obtained by applying a function (CTI.aml) compiled by USDA Forest Service Rocky Mountain Research Station to the 1 km GTOP30 elevation dataset. The global CTI was produced by combining the two datasets and then transformed it to 30 arc-second resolution.

$$\mathrm{CTI} = \ln\left(\frac{A_S}{\tan\beta}\right), \tag{1}$$

where A_S is the flow accumulation and β is the slope in radians.

The datasets used to drive the water balance model are

the average monthly climate data at 5min resolution during 1950–2000. These datasets were obtained from WorldClim (http://www.worldclim.org/), including average monthly precipitation, average monthly maximum temperature, and average monthly minimum temperature.

To acquire global wetland samples, we collected five global land cover products and seven regional land cover products for 2000 (Table 1). From Table 1 we can see that there is a distinct disagreement in wetland definitions. We extracted wetland areas from these land cover products according to the wetland definition in Ramsar Convention. Wetland definition in Ramsar Convention contains not only swamps, estuaries, peat lands, and mangroves but also lakes, rivers, alpine meadows, and tundra. Among the five global land cover datasets, GLWD was specially oriented to wetland and included 12 wetland types, so all of the area was classified as wetland. GLC2000 was accomplished based on cooperation with various institutes so the wetland definition also varied in space. We classified all land cover types in accordance with the wetland definition in the Ramsar Convention (Table 1). Land cover types like water bodies, herbaceous wetlands, wooded wetlands, herbaceous tundra, wooded tundra, and mixed tundra in IGBP-DISCover were all classified as wetland. In GLCNMO and the MODIS product, land cover types that could be regarded as wetland only include water bodies and permanent wetlands. Apparently, these datasets are comparable, because they can be unified under the framework of wetland definition in Ramsar Convention.

To unify these datasets with different resolutions, all of these datasets were resampled to 1 km. In the process of resampling from the higher resolution datasets, land cover categories were aggregated into 1 km pixels. Only pixels whose proportion of wetlands exceeds 80% were categorized as wetland to keep purity of wetland samples. To ensure accuracy among wetland samples, we took the intersection among different wetland datasets as wetland samples. Meanwhile, water bodies were eliminated from the intersection dataset to adjust for the proportion of water samples in wetland samples. Water samples were taken from the global water body dataset MODIS Water Mask (MWM) that was obtained from http://glcf.umd.edu/data/watermask/. In order to ensure the quality of no wetland samples, we took the union of all wetland extents from different datasets and then added a buffer zone of 5 km to get the maximum possible extent of wetlands. Random sample points of no wetland were extracted with HawthsTools in ArcGIS from areas outside the unified and buffered wetland areas. Because the area of the intersection and water-eliminated wetland extent was already rather small, we collected 75000 wetland sample points accounting for approximately 30% of the total intersected wetland area and collected 10000 water sample points from the MWM. Nine thousands of no wetland points were extracted. To evaluate the quality of the wetland samples, 4000 points were randomly drawn from the wetland samples. From Google Earth high resolution images, we located the 4000 samples and checked if they are indeed wetlands. Only 67 points could not be confirmed as wetland, indicating that the wetland sample has high certainty.

Table 1 Characteristics of the five global land cover datasets and products and seven regional land cover products

Land cover product	Data used	Data collection period	Classification system	Resolution (km)	Classification
Global scale					
IGBP-DISCover	NOAA-AVHRR image	1992–1993	IGBP (17 classes)	1	Unsupervised clustering
BU-MODIS	Terra MODIS	2000–2001	IGBP (20 classes)	1	Supervised decision tree
GLC2000	SPOT Vegetation	1999–2000	FAO LCCS (23 classes)	1	Flexible classification depending on the institutions
GLCNMO	Terra MODIS	2003	FAO LCCS (23 classes)	1	Supervised classification tree
GLWD	Wetland map, GLCC, DCW DNNE	1992–1993	12 wetland classes	1	–
Regional scale					
USA National wetlands Inventory	Aerial photography draft map, field investigation	—	Wetland/no wetland	1:144000	High altitude image in conjunction with collateral data sources and field work
Canada Circa 2000-Vector land cover datasets	Landsat	1999–2002	Author's own	30 m	Clustering
China wetland	Landsat TM ETM	2000	Author's own	30 m	Manual interpretation
Europe CORINE Land Cover 2000	Landsat-7 ETM	1999–2001	Author's own	100 m	Manual interpretation and automated classification
Amazon basin wetland mask	JERS-1 SAR image data	1995–1996	Wetland/No wetland	100 m	polygon-based segmentation and clustering process
Australia landcover	MODIS 16-day EVI composite	2000–2008	Author's own	250 m	Support vector clustering
AfriCover	TM	2000s	FAO LCCS (23 classes)	30 m	Manual interpretation

The development mechanism of land surface wetland varied across different areas. In particular, climatic factors determine the way of water provision to land surface wetland under different climate conditions. According to different climate systems and wetting mechanisms, wetlands at different areas are divided into four types: (1) mostly precipitation and local runoff-fed, such as bogs and marshland which are disconnected from river networks; (2) mostly surface water-fed but groundwater-supported, such as coastal freshwater wetlands, tropical-subtropical forests and inland floodplains; (3) mostly groundwater fed, such as inland freshwater wetlands in semi-arid climate areas; and (4) mostly frozen ground-supported (Fan and Miguez-Macho, 2011). According to these hydrological mechanisms, it is necessary to model wetlands in different climate zones with different parameters. Freshwater Ecoregions of the World (FEOW) (http://www.feow.org/) were used to construct the units within each of which model parameters are established. The FEOW were developed for freshwater biodiversity conservation. They were produced mainly based on drainage basin boundaries. The comparison between this dataset and another global basin dataset, USGS HydroSHEDS, showed a good spatial agreement. FEOW contained 426 regions, and we selected six bioclimatic variables: annual mean temperature, maximal temperature of warmest month, minimal temperature of coldest month, annual precipitation, precipitation of wettest month, and precipitation of driest month from WorldClim and calculated the average of these variables for each region as its feature variables. These feature variables were then standardized by subtracting the average value and divided by the standard deviation. Finally a *k*-means clustering algorithm was applied to the 426 regions using the six feature variables as inputs to generate 15 climatic-basin clusters (Figure 1), which were used as our modeling units. The comparison between our climate-basin clusters and Köppen Climate Classification System indicates that our clustering results not only can reflect the geographical distribution of global climatic regions but also can distinguish hydrological controls of basins in different wetland ecosystems.

1.2 Modeling the distribution of soil water content

Our model runs at monthly time interval. With the deficiency of high resolution climatic forcing datasets the calculation of soil water content was based on a simple water balance model including the processes of precipitation, evapotranspiration, and runoff generation but ignoring the processes of vegetation interception, interaction between land surface water and underground water (recharge and discharge). The soil water content was updated monthly:

$$P(t) - ET(t) - R(t) = \frac{\mathrm{d}W(t)}{\mathrm{d}t}, \tag{2}$$

where $P(t)$, $ET(t)$, $R(t)$, and $W(t)$ refer to precipitation, evapotranspiration (ET), runoff, and soil water content at time t, respectively. The calculated soil water content in eq. (2) should be viewed as the average soil water content in a 5 min grid cell rather than the rigid definition of soil water content in pedology. ET was calculated based on the hypothesis that it has a direct proportional relationship with the relative soil water content and potential evapotranspiration (PET) (Prentice et al., 1993):

$$ET(t) = PET(t)w_{\mathrm{std}}, \tag{3}$$

$$w_{\mathrm{std}} = \frac{W(t) - w_{\mathrm{wilt}}}{w_{\mathrm{sat}} - w_{\mathrm{wilt}}}. \tag{4}$$

where w_{sat}, w_{wilt}, and w_{std} respectively refer to soil permanent wilting point, soil porosity, and relative soil water content. The basic soil datasets were obtained from Harmonized World Soil Database v1.2 (http://webarchive.iiasa.ac.at/Research/LUC/External-World-soil-database/HTML/). Soil

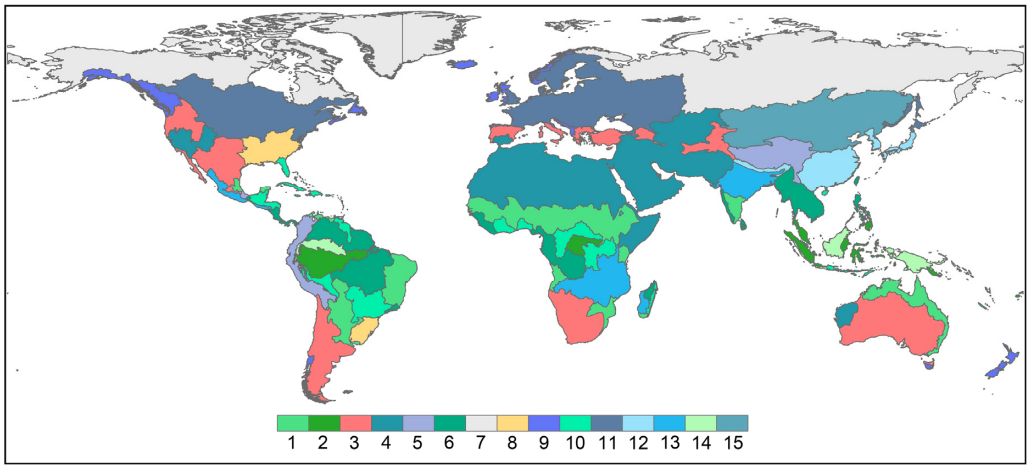

Figure 1 Fifteen climatic-basin clusters based on bioclimatic variables.

permanent wilting point and soil porosity were determined using the same parameters in NOAH (National Centers for Environmental Prediction Oregon State University Air Force Hydrologic Research Lab) to keep consistent with NOAH output variables (Ek et al., 2003). The soil parameters are listed in Table 2. PET was calculated following Hargreaves and Samani (1985).

To quantify the impact of surface runoff on soil water content, we used the following parameterization scheme which was expressed as the function of precipitation and relative soil water content (Bergstrom, 1995):

$$R(t) = P(t)w_{\text{std}}^{\alpha}, \tag{5}$$

where α was solved using 0–2 m depth soil water content data in NOAH LSM offered by Global Land Data Assimilation System (GLDAS). NOAH LSM is an operational LSM coupling physical processes of the soil-vegetation-atmosphere and characterizing the land surface process more accurately than our model, but its coarse spatial resolution prevents it from being used in high resolution wetland modeling. Therefore, we got each month's mean soil water content by averaging NOAH output soil water content datasets for 1950–2000 and then solved parameter α with eqs. (2) and (5). α is viewed as a temporally invariable and scale-independent parameter reflecting the nature of basins. Finally, with the solved α our model ran for 30 times to reach a steady state and then got the soil water content at 5 min resolution. Thirty times were chosen because it produced stabilizing soil water content result. Following eq. (4), we could calculate the average value of relative soil water content for 1950–2000, which is shown in Figure 2.

1.3 Determination of land surface wetland distribution based on water table depth

Under the TOPMODEL assumptions that the surface infiltration rate and soil properties are uniform across a basin and that subsurface transmissivity has an exponential profile with water table depth, the local water table depth wtd_i at position i within a 5-min grid cell can be expressed as a function of the average grid cell water table and grid cell topography (Beven and Kirkby, 1979):

$$\overline{\text{wtd}} - \text{wtd}_i = -M(\bar{\lambda} - \lambda_i) \tag{6}$$

where $\overline{\text{wtd}}$ is the mean water table depth (WTD) of the 5 min grid cell, λ_i is the local CTI index at i, $\bar{\lambda}$ is the mean CTI, and M is a scaling parameter. While eq. (6) is established over an entire basin, rather than a grid cell, the 5 min grid cells we used are sufficiently large so that the relationship can hold approximately true, i.e., pixels for which a significant fraction of their upslope contributing area lies outside the cell boundaries make up only a small fraction of the grid cell (Bohn et al., 2007).

Table 2 Soil parameters corresponding to various soil texture class

Soil texture class	Permanent wilting point	Soil porosity
Sand	0.339	0.236
Loamy sand	0.421	0.383
Sandy loam	0.434	0.383
Silt loam	0.476	0.360
Silt	0.476	0.383
Loam	0.439	0.329
Sandy clay loam	0.404	0.314
Silt clay loam	0.464	0.387
Clay loam	0.465	0.382
Sandy clay	0.406	0.338
Silt clay	0.468	0.404
Clay	0.468	0.412

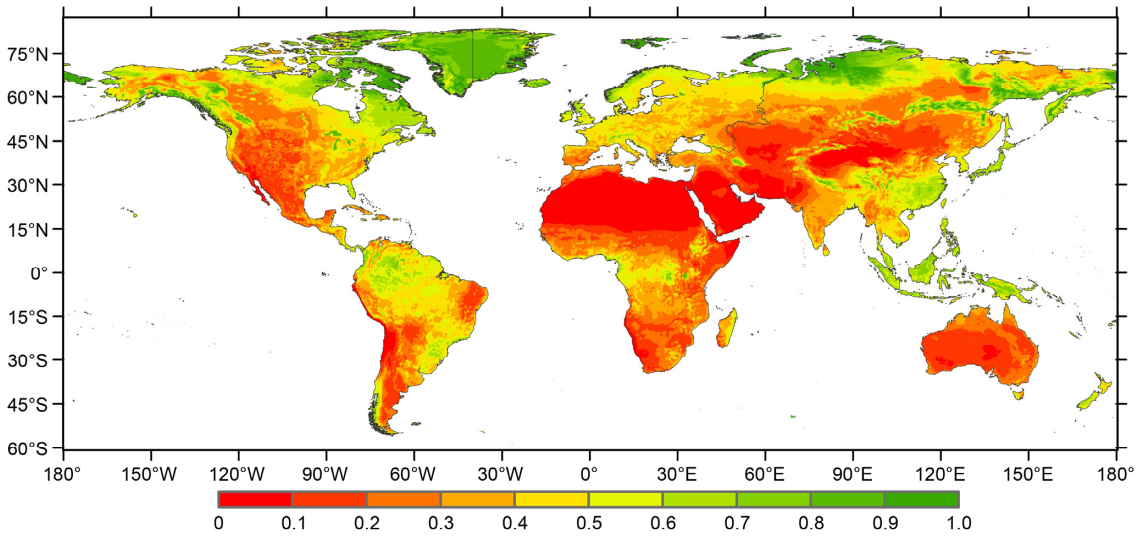

Figure 2 Average value of relative soil water content for 1950–2000.

Before acquiring WTD at each point, we must get the mean WTD of 5 min grid cell. For peat land area (Hilbert et al., 2000), we can use the following equation:

$$\mathrm{ET} = \frac{\mathrm{PET}}{1 + c \cdot \overline{\mathrm{wtd}}}. \quad (7)$$

Then the relation between w_{std} and $\overline{\mathrm{wtd}}$ can be denoted as

$$w_{\mathrm{std}} = \frac{1}{1 + c \cdot \overline{\mathrm{wtd}}}, \quad (8)$$

where c is a parameter to be determined. Finally wtd_i can be expressed as

$$\mathrm{wtd}_i = \frac{1 - w_{\mathrm{std}}}{c w_{\mathrm{std}}} + M(\bar{\lambda} - \lambda_i). \quad (9)$$

The above equation shows that as long as parameters c and M are determined, the global WTD at each point can be solved. However, it is hard to get accurate values for the two parameters globally. Since the result we need is wetland distribution rather than a global WTD map, we proposed the following method to determine the global land surface wetland distribution by using an optimal threshold that distinguishes the wetland from no wetland area.

The wetland and no wetland sample points were used as binary variable (B) to calibrate parameters c and M (when it is wetland, B=1; otherwise B=0). We introduced a sigmoidal function, $f(\mathrm{wtd}_i) = 1/1 + \mathrm{e}^{-\mathrm{wtd}_i}$, which could map wtd_i into 0–1 to relate B with wtd_i. $\min\delta$ was used as the solving condition where

$$\delta = \sum (B - f(\mathrm{wtd}_i))^2. \quad (10)$$

Parameters c and M were individually solved for 15 global climatic-basin regions, given that values of these parameters varied across different climate zones (Table 3). To quantify the optimal WTD thresholds to distinguish wetland suitability areas, wetland and no wetland samples were used as validation data to determine the accuracy with different WTD as thresholds. Finally, the corresponding WTDs with the highest accuracy achieved were chosen as the optimal thresholds to distinguish wetland from no wetland area (Table 3).

Table 3 c, M and optimal WTD thresholds for different climatic-basin regions

Climatic-basin regions	c	M	Optimal WTD thresholds (m)
1	105.26	0.494	–0.435
2	34.25	0.357	–0.237
3	8.83	0.322	–0.359
4	178.57	0.39	–0.777
5	34.96	0.564	–0.213
6	2.01	0.505	–0.368
7	1.82	0.257	–0.426
8	9.95	0.483	–0.468
9	0.89	0.262	0.040
10	1.50	0.626	–0.447
11	2.27	0.351	–0.116
12	0.51	0.644	–0.223
13	3.20	0.636	–0.549
14	0.92	0.465	–0.205
15	4.85	0.433	1.000

2 Results and discussion

Based on water cycling process and the relation between WTD and wetlands, the global land surface wetland suitability map was produced (Figure 3). A recent study produced a global pattern of WTD through numerically solving Darcy's law and Richards equation (Fan et al., 2013). In their study, 0.25 m was used as the threshold to distinguish wetland from no wetland areas. Since their study did not account for human activities either, their result can also be viewed as a wetland suitability map (Figure 4). The comparison between these two global wetland suitability maps exhibited a good spatial agreement. Our modeling result indicates that the total area of global land surface wetland is 3.316×10^7 km^2, and Fan's result is 3.376×10^7 km^2. The two results were aggregated to 5 min resolution to get the proportion of wetland at each grid cell. The difference between the two maps indicated that the major area of disagreement was located in the Northern Hemisphere especially at high latitudes such as northern Canada, West Siberia, and Northeast China (Figure 5). The differences are caused by the different models employed and the different topographical data used at greater than 60°N.

Wetland and no wetland samples greater than 1 km were compiled from the validation dataset of our global land cover mapping project (Gong et al., 2013). Since the number of wetland samples selected from this datasets was much smaller than that of no wetland points, internationally important wetland points from Ramsar Convention were added to form a validation datasets consisting of 8112 wetland samples and 12358 no wetland samples. This validation dataset was used to assess the accuracy of our modeling result, Fan's result, and the five global land cover mapping based on remotely sensed images. The confusion matrix (Table 4) indicates that our result has produced a higher accuracy in both Producer's Accuracy (PA) and User's Accuracy (UA) than did Fan's result. The Overall Accuracy (OA) of our result is 83.7%, which is the highest among all datasets. This indicates our result holds a great potential to serve as a guide to constructing global wetland databases. Latitudinal distributions of area fraction for the seven global wetland maps (our result, Fan's result, and five remote sensing based wetland mapping) show a consistent spatial pattern (Figure 6). In areas largely impacted by human activities

(about 40°S–55°N), model-based results have a larger wetland area fraction than the other five remote-sensing-based wetland map results and in areas less impacted by human activities (about above 55°N), model-based wetland area fractions are in the middle of this range. There are two regions with plentiful wetlands along the global latitudinal distribution: regions along the equator and regions along the 60°N.

An area comparison among the seven global wetland results shows that our result contains similar wetland area to Fan's modeling result (Table 4) but both are greater than the areas in the five remote sensing based maps. The wetland areas in BU-MODIS and GLCNMO are much smaller than the areas in the modeled wetlands. The main reasons are: (1) BU-MODIS and GLCNMO wetland extents only include permanent wetland and water bodies; although the other three wetland extents include floodplain, and the maximum extent of short-term inundation is hard to capture from a single date remotely sensed image. This is especially true for highly varying seasonal lakes like the Poyang Lake and the ratio between the maximum and minimum inundation areas could be greater than three (Sun et al., 2014). Thus, wetland maps derived from a single date remote sensing images tend to underestimate wetland areas. However, wetland areas determined by modeling topographic and hydrologic processes usually include most areas suitable to wetland development. Therefore, they are likely to overestimate wetland areas. (2) Neither of the two model-derived results accounted for impact of anthropogenic water management such as irrigation and reservoir development on wetlands. We did not include anthropogenic water management in our study because we do not have the related human activities data. Lacking such data is also the main difficulties in large scale hydrological modeling (Pokhrel et al., 2012; Wood et al., 2011). Moreover, a larger wetland suitability area could serve as a guide to more accurate wetland mapping using remote sensing because areas outside the wetland suitability mask could be ignored to reduce errors caused by spectral confusion.

For coastal wetlands, there is a large variation in width of wetland zone along the coastal line as determined by various topographic structures and subtle surface relief. Such variations cannot be fully captured in coarse resolution DEM datasets as the ones we used. Therefore, we concentrated our research on land surface wetland suitability mapping to reduce uncertainty. The model used here is relatively simple as compared to those used by Fan and WETCHIMP but it showed a better performance in mapping suitable wetlands in accuracy based on our validation. We attribute the better performance of our method partially to the adoption of climatic-basin units within which unique model parameters are applied. Another reason is that it incorporated

Table 4 Accuracy and area comparison across seven global wetland results

This result	Wetland	No wetland	PA (%)	UA (%)	Overall accuracy (%)	Wetland area (10^6 km^2)
Wetland	5915	1830	80.7	76.4	83.7	33.16
No wetland	1414	10779	85.5	88.4		
Fan's result						
Wetland	5150	2632	75.2	66.2	78.3	33.76
No wetland	1702	10516	80.0	86.1		
IGBP-DISCover						
Wetland	4678	5879	86.9	44.3	71.3	32.47
No wetland	702	11655	66.5	94.3		
GLWD						
Wetland	5457	5100	85.8	51.7	73.8	25.63
No wetland	901	11456	69.2	92.7		
GLC2000						
Wetland	5158	5399	83.3	48.9	71.9	26.86
No wetland	1035	11322	67.7	91.6		
GLCNMO						
Wetland	3706	6851	95.0	35.1	69.3	6.40
No wetland	196	12161	64.0	98.4		
BU-MODIS						
Wetland	4563	5994	97.1	43.2	73.2	7.81
No wetland	137	12220	67.1	98.9		

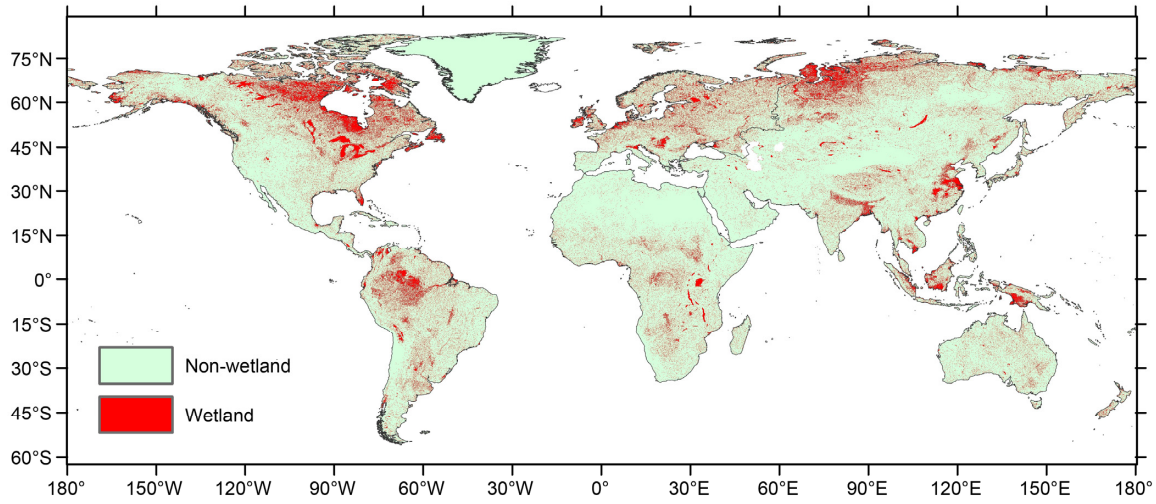

Figure 3 Global wetland suitability modeling result in this study.

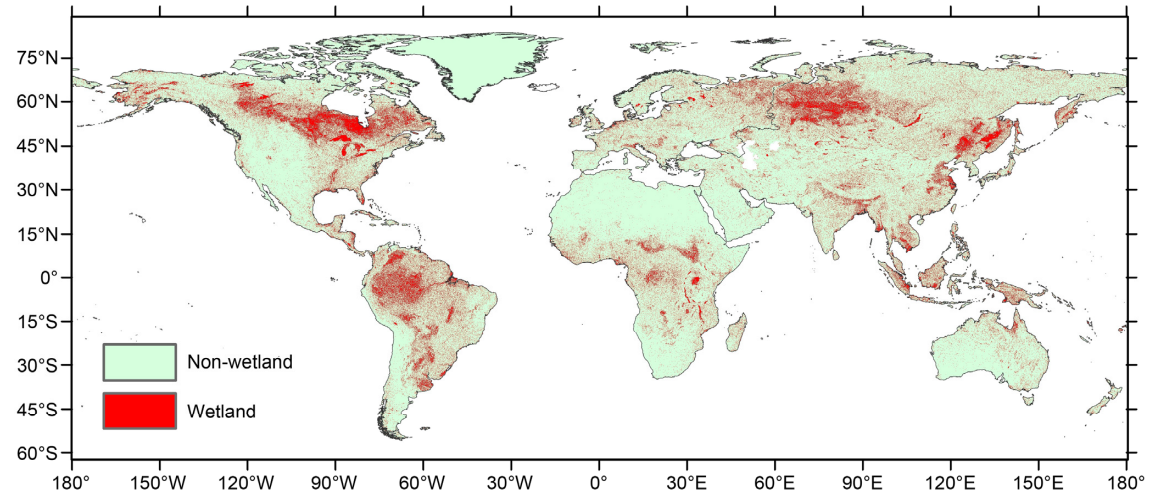

Figure 4 Global wetland modeling result derived from Fan's result (2013).

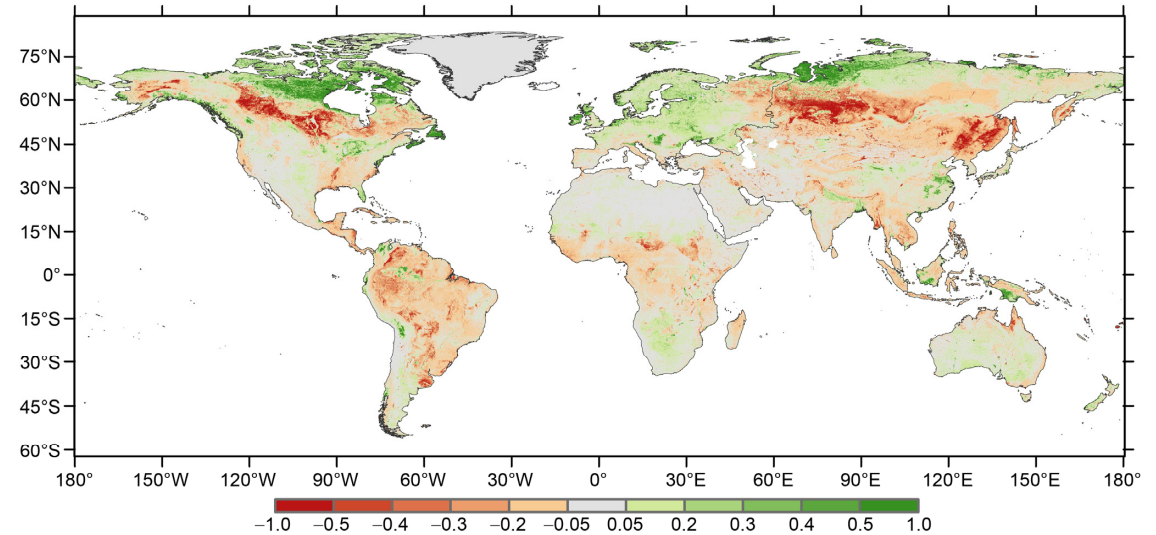

Figure 5 The difference of wetland proportion between our modeling result and Fan's at each 5 min grid cell.

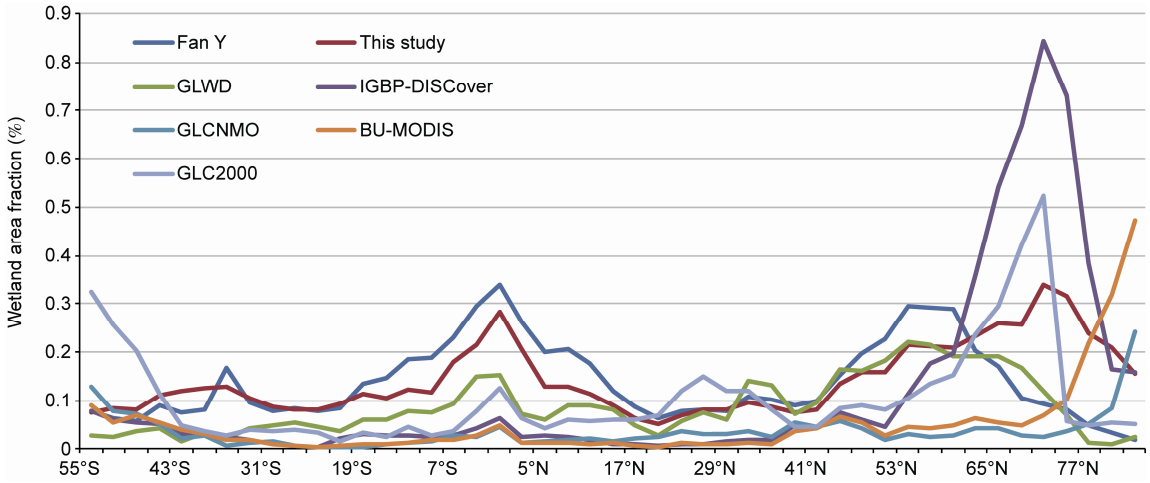

Figure 6 Latitudinal distribution of seven global wetland area fraction.

the soil water content datasets from NOAH, which have demonstrated good quality in other research (Rodell et al., 2007; Syed et al., 2008; Zhang et al., 2008). Our result also proves that exploring and modeling global wetland at high resolution from a water cycling perspective is feasible. Since we did not account for the impact of human-induced disturbance to the natural water cycling, our result overestimated the area of global wetland. In the future we expect that more human impact factors will be represented and more hydrological processes will be included into land surface models to produce more accurate global wetland distribution data.

This work was supported by National High-tech R&D Program of China (Grant No. 2009AA12200101).

Bartholomé E, Belward A. 2005. GLC2000: A new approach to global land cover mapping from Earth observation data. Int J Remote Sens, 26: 1959–1977

Bergstrom S. 1995. The HBV Model. In: Singh V P, ed. Computer Models of Watershed Hydrology. Colorado: Water Resources Publications. 443–476

Beven K, Kirkby M. 1979. A physically based, variable contributing area model of basin hydrology. Hydrol Sci J, 24: 43–69

Bohn T J, Lettenmaier D P, Sathulur K, et al. 2007. Methane emissions from western Siberian wetlands: Heterogeneity and sensitivity to climate change. Environ Res Lett, 2: 045015

Decharme B, Douville H. 2006. Introduction of a sub-grid hydrology in the ISBA land surface model. Clim Dyn, 26: 65–78

Decharme B, Douville H. 2007. Global validation of the ISBA sub-grid hydrology. Clim Dyn, 29: 21–37

Dronova I, Gong P, Wang L. 2011. Object-based analysis and change detection of major wetland cover types and their classification uncertainty during the low water period at Poyang Lake, China. Remote Sens Environ, 115: 3220–3236

Ek M, Mitchell K, Lin Y, et al. 2003. Implementation of the upgraded Noah land-surface model in the NCEP operational mesoscale Eta model. J Geophys Res, 108: 8851

Fan Y, Miguez-Macho G. 2011. A simple hydrologic framework for simulating wetlands in climate and earth system models. Clim Dyn, 37: 253–278

Fan Y, Li H, Miguez-Macho G. 2013. Global patterns of groundwater table depth. Science, 339: 940–943

Friedl M, McIver D, Hodges J, et al. 2002. Global land cover mapping from MODIS: Algorithms and early results. Remote Sens Environ, 83: 287–302

Gong P, Niu Z G, Cheng X, et al. 2010. China's wetland change (1990–2000) determined by remote sensing. Sci China Earth Sci, 53: 1036–1042

Gong P, Wang J, Yu L, et al. 2013. Finer resolution observation and monitoring of global land cover: First mapping results with Landsat TM and ETM+ data. Int J Remote Sens, 34: 2607–2654

Habets F, Saulnier G M. 2001. Subgrid runoff parameterization. Phys Chem Earth Pt B, 26: 455–459

Hargreaves G H, Samani Z A. 1985. Reference crop evapotranspiration from ambient air temperature. Appl Eng Agric, 1: 96–99

Hilbert D W, Roulet N, Moore T. 2000. Modelling and analysis of peatlands as dynamical systems. J Ecol, 88: 230–242

Hui F, Xu B, Huang H, et al. 2008. Modelling spatial-temporal change of Poyang Lake using multitemporal Landsat image. Int J Remote Sens, 29: 5767–5784

Ji W, Zeng N, Wang Y, et al. 2007. Analysis on the waterbirds community survey of Poyang Lake in winter. Geogr Inf Sci, 13: 51–64

Lehner B, Döll P. 2004. Development and validation of a global database of lakes, reservoirs and wetlands. J Hydrol, 296: 1–22

Loveland T, Reed B, Brown J, et al. 2000. Development of a global land cover characteristics database and IGBP DISCover from 1 km AVHRR data. Int J Remote Sens, 21: 1303–1330

Melton J R, Wania R, Hodson E L, et al. 2013. Present state of global wetland extent and wetland methane modelling: Conclusions from a model inter-comparison project (WETCHIMP). Biogeosciences, 10: 753–788

Nakaegawa T. 2012. Comparison of water-related land cover types in six 1-km global land cover datasets. J Hydrometeorol, 13: 649–664

Niu Z G, Gong P, Cheng X, et al. 2009. Geographical characteristics of China's wetlands derived from remotely sensed data. Sci China Ser D-Earth Sci, 52: 723–738

Niu Z G, Zhang H Y, Wang X W, et al. 2012. Mapping wetland changes in China between 1978 and 2008. Chin Sci Bull, 57: 2813–2823

OECD. 1996. Guidelines for aid agencies for improved conservation and sustainable use of tropical and subtropical wetlands. Organization for Economic Co-operation and Development, Paris, France

Pokhrel Y, Hanasaki N, Koirala S, et al. 2012. Incorporating anthropogenic water regulation modules into a land surface model. J Hydrometeorol, 13: 255–269

Prentice I C, Sykes M T, Cramer W. 1993. A simulation-model for the transient effects of climate change on forest landscapes. Ecol Model, 65:

51–70
Ringeval B, Decharme B, Piao S L, et al. 2012. Modelling sub-grid wetland in the ORCHIDEE global land surface model: Evaluation against river discharges and remotely sensed data. Geosci Model Dev, 5: 683–735
Rodell M, Houser P, Jambor U, et al. 2004. The global land data assimilation system. Bull Amer Meteorol Soc, 85: 381–394
Rodell M, Chen J, Kato H, et al. 2007. Estimating groundwater storage changes in the Mississippi River basin (USA) using GRACE. Hydrogeol J, 15: 159–166
Sun F D, Zhao Y Y, Gong P, et al. 2013. Monitoring dynamic changes of global land cover types: Fluctuations of major lakes in China every 8 days from 2000–2010. Chin Sci Bull, 59: 171–189
Syed T H, Famiglietti J S, Rodell M, et al. 2008. Analysis of terrestrial water storage changes from GRACE and GLDAS. Water Resour Res, 44: W02433
Tateishi R, Uriyangqai B, Al-Bilbisi H, et al. 2011. Production of global land cover data—GLCNMO. Int J Digit Earth, 4: 22–49
Wilen B, Bates M. 1995. The US fish and wildlife service's national wetlands inventory project. Vegetatio, 118: 153–169
Wood E F, Roundy J K, Troy T J, et al. 2011. Hyperresolution global land surface modeling: Meeting a grand challenge for monitoring Earth's terrestrial water. Water Resour Res, 47: W05301
Zedler J B, Kercher S. 2005. Wetland resources: status, trends, ecosystem services, and restorability. Annu Rev Environ Resour, 30: 39–74
Zhang J, Wang W C, Wei J. 2008. Assessing land-atmosphere coupling using soil moisture from the Global Land Data Assimilation System and observational precipitation. J Geophys Res, 113: D17119
Zheng Y M, Zhang H Y, Niu Z G, et al. 2012. Protection efficacy of national wetland reserves in China. Chin Sci Bull, 57: 1116–1134